

Deformation and Structural Stability of Layered Plate Microstructures Subjected to Thermal Loading

Martin L. Dunn, Yanhang Zhang, and Victor M. Bright, *Member, IEEE*

Abstract—We study the deformation and stability of gold–polysilicon MEMS plate microstructures fabricated by the MUMPS surface micromachining process and subjected to uniform temperature changes. We measured, using an interferometric microscope, full-field deformed shapes of a series of square and circular gold (0.5 μm thick)/polysilicon (1.5 μm thick) plate microstructures with characteristic lengths l (square side length and circle diameter) ranging from $l = 150$ to $300 \mu\text{m}$. From these measurements we determined the pointwise and average curvature of the deformed plates. Although the curvature generally varies with position, the deformation response of the plates can be broadly characterized in terms of the spatial average curvature as a function of temperature change. In terms of this, three deformation regimes were observed: i) linear thermoelastic response independent of plate size; ii) geometrically nonlinear thermoelastic response that depends on plate size; and iii) bifurcations in the curvature-temperature response that also depend on plate size. We modeled the deformation response both analytically and with the finite element method; in the former we assume spatially constant curvature, while in the latter, we relax this assumption. Good qualitative and quantitative agreement is obtained between predictions and measurements in all three deformation regimes, although the details of bifurcation are less accurately predicted than the linear and nonlinear response. This is attributed to their strong sensitivity to slight imperfections, which is discussed in some detail. Good agreement is also obtained between measurements and predictions of the spatial nonuniformity of the curvature across the plate. Although it is not the focus of this study, the predictions, when coupled with curvature measurements, can be used inversely to determine elastic and thermal expansion properties of the materials in a layered plate microstructure. [677]

I. INTRODUCTION

MULTILAYER material systems abound in microelectromechanical systems (MEMS) applications, serving both active and passive structural roles. In these many applications, dimensional control is a critical issue. Surface micromachined mirrors, for example, require optically flat surfaces; less than 10% of a wavelength variation across the mirror's surface. Holographic data storage and optical beam steering for display applications need reflective surfaces free of optical phase distortion to increase the signal-to-noise ratio, minimize crosstalk, and keep the system in focus. This level of optical flatness is difficult to achieve due to curvature

commonly seen in micromachined mirrors composed of several different material layers. For other applications, such as radio frequency (RF) MEMS, cantilever and bridge like structures are used to make electrostatic switches. It is important to control warpage of these large area, thin actuator structures in order to achieve desired deflection versus voltage relationships, on–off switching times, and RF frequency response. An inherent characteristic of such multilayer material structures is that misfit strains between the layers (for example, due to intrinsic processing stresses or thermal expansion mismatch between the materials upon a temperature change) lead to stresses in the layers and deformation of the structures.

Numerous studies have elucidated the basic thermomechanical response of layered plates when subjected to temperature changes or other sources of misfit strains between the layers. These have come in the context of many technological applications, the most common being structural composite materials (Hyer, [16]–[18]; Dano and Hyer, [2]) and thin film/substrate systems for microelectronics (Fahnline *et al.*, [7]; Masters and Salamon, [22]; Finot and Suresh, [8]; Finot *et al.*, [9]; Freund, [10]–[12], [14]; Freund *et al.*, [13]). When such a layered plate is subjected to a temperature change, two key aspects of deformation occur: straining of the midplane and bending. When the transverse deflections due to bending are of prime importance, as is often the case, one way to broadly characterize the deformation response, especially for plates with relatively large in-plane dimensions as compared to their thickness, is in terms of the average curvature developed as a function of temperature change. Formally, the curvature is a second-rank tensor, and for the type of layered plate problems considered here it can be wholly described by the two principal curvature components, e.g., in the x - and y - directions, κ_x and κ_y . The curvature is a pointwise quantity meaning it varies from point to point over the in-plane dimensions of the plate. To illustrate the nature of deformation, we consider the seemingly simple case of a plate with total thickness much less than the in-plane dimensions of the plate composed of two isotropic layers with different material properties (elastic modulus and thermal expansion) subjected to a temperature change (Fig. 1(a)). In terms of the average curvature variation as a function of temperature change, three deformation regimes have been identified as illustrated in Fig. 1(b) (Finot and Suresh, [8], Finot *et al.*, [9], Freund *et al.*, [13]; Freund, [14]; Masters and Salamon, [22], [23]; Salamon and Masters, [24]). The first regime, *I*, consists of a linear relation between the average curvature and temperature change where $\kappa_x = \kappa_y$, i.e., the average curvature is spherically symmetric. This symmetric deformation would not exist if the material properties were anisotropic. This deformation

Manuscript received March 27, 2001; revised November 9, 2001. This work was supported by the Defense Advanced Research Projects Agency (DARPA) and the Air Force Research Laboratory, Air Force Material Command, USAF, under agreement F30602-98-1-0219. Subject Editor D. Cho.

The authors are with the Department of Mechanical Engineering, University of Colorado at Boulder, Boulder, CO 80309 USA (e-mail: Martin.Dunn@colorado.edu).

Publisher Item Identifier 10.1109/JMEMS.2002.800932.

regime is characterized by both small transverse displacements and rotations and so conventional thin-plate theory adequately describes the deformation. The second regime, *II*, consists of a nonlinear relation between the average curvature and temperature, but again $\kappa_x = \kappa_y$. The behavior is due to *geometric non-linearity* that results when the deflections become excessively large relative to the plate thickness and they contribute significantly to the in-plane strains. It has been shown (Fahnline *et al.*, [7]; Finot and Suresh, [8]; Finot *et al.*, [9]; Freund *et al.*, [13]; Freund, [14]; Masters and Salamon, [22], [23]; Salamon and Masters, [24]) that in these two regimes the symmetric deformation modes are stable. The second regime ends at a point when the deformation response bifurcates from a spherical to ellipsoidal deformation, i.e., $\kappa_x \neq \kappa_y$. At this point, the beginning of regime *III*, it becomes energetically favorable for the plate to assume the ellipsoidal shape because to retain the spherical deformation under an increasing temperature change require increased midplane straining. After the bifurcation the curvature in one direction increases while that perpendicular to it decreases; the plate tends toward a state of cylindrical curvature. This observation helps to explain the energetic argument as unlimited cylindrical curvature can be obtained with no mid-plane straining, while spherical curvature can not. This discussion has been cast in the context of linear material behavior. Additional deformation regimes result if material nonlinearity is present, for example, yielding, but these are beyond the scope of this work (see Finot and Suresh, [8], for a discussion of some of these issues).

Most previous work regarding the deformation of layered systems has focused on the first linear regime. This includes most of the understanding developed in the context of microelectronics applications where the thin film limit of this behavior is applicable. Indeed, much of the understanding of these issues in MEMS applications is built upon this knowledge base. In this case one layer (the thin film) is much smaller than the other (the substrate). A 0.5- μm -gold film on a 500- μm -thick, 100-mm-diameter silicon substrate is a reasonable example. If subjected to a 100 °C temperature change, the maximum deflection would about two percent of the thickness if the film fully covered the substrate, and even less if it were patterned discontinuously. The deformation falls into the linear regime *I* of Fig. 1(b). In fact, the most common application of this behavior in microelectronics is the use of the Stoney [28] equation to determine thin film stresses (which are typically biaxial and spatially uniform) from measured wafer curvature. In MEMS applications the layer thicknesses are not only small (on the order of μm) relative to in-plane dimensions, but they are often comparable to each other. An example that is not unreasonable is a 0.5- μm gold film on a 1.5- μm -thick, 400- μm -diameter polysilicon plate. If subjected to a 100°C temperature change, the maximum deflection would be about six times of the thickness. This falls into the nonlinear second regime *II* of Fig. 1(b), and perhaps even into regime *III*. Although not as heavily studied as the first, the second and third deformation regimes have been observed in structural composites cured at elevated temperatures (Hyer, [16]), and more recently in microelectronics thin film systems (Finot *et al.*, [9]) and MEMS microstructures intended for RF applications (Harsh *et al.*, [5]; Dunn *et al.*, [4]). While much of

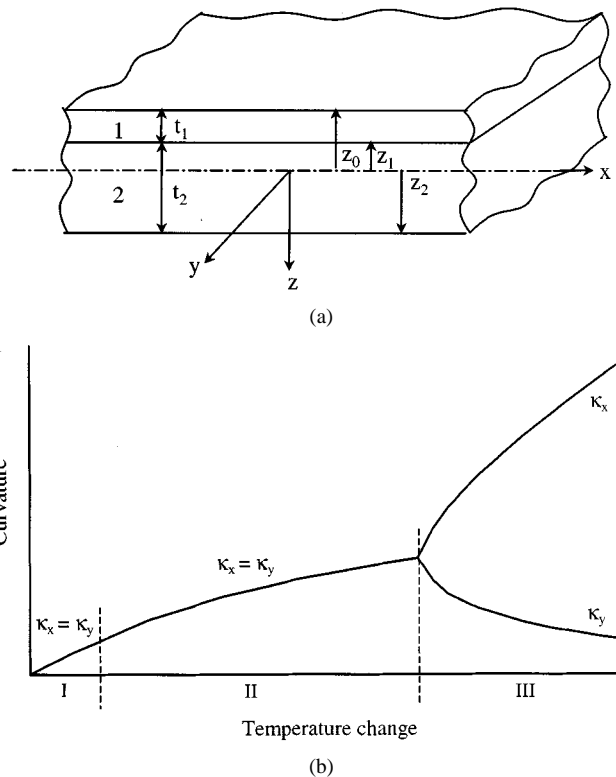


Fig. 1. Schematic of (a) the geometry of the two-layer plate microstructure showing relevant dimensions, and (b) the general characteristics of the average curvature versus temperature change of a two-layer plate microstructure.

the understanding regarding the thermomechanical behavior of layered systems derives from experiences in microelectronics, a key aim of this paper is to point out that significant differences exist for many MEMS applications, and these must be well understood to optimize the design of reliable MEMS.

The understanding described above derives from a number of studies with different technological motivations, primarily structural laminated composites and thin films for microelectronics. Most of these studies are analytical (Fahnline *et al.*, [7]; Finot and Suresh, [8]; Finot *et al.*, [9]; Freund *et al.*, [13]; Freund, [14]; Harper and Wu, [15]; Masters and Salamon, [22], [23] Salamon and Masters, [24]) and build upon the original work of Hyer [16]–[18]. The basic idea of Hyer's, and all of the subsequent, analyses is to assume an admissible displacement field $w(x, y)$ in terms of unknown parameters (d_i) that are suitably chosen to be consistent with observed deformation modes. Values of the parameters d_i are then determined via a Ritz procedure so as to minimize the total potential energy of the system. Different choices of the assumed displacement field have been considered by these authors, and details of the procedures are given in the above references. Such analyses are sufficient to qualitatively, and in many cases quantitatively, explain the three regimes of deformation shown in Fig. 1(b). In fact, quite simple closed-form expressions result for special cases that provide illuminating descriptions of observed phenomena (see, for example, Freund *et al.*, [13] and Freund [14]). A disadvantage of the analytical approaches is that for simplicity a displacement field that is consistent with a spatially constant curvature deformation mode is usually chosen. As will be seen in our measurements and calculations, this is accurate in certain

deformation regimes, but not in all. Additionally, these formulations are strictly valid for only simple plate shapes; this may be adequate for the structures considered here, but it is not for more complex in-plane shapes, of either or both layers, that arise in MEMS applications (see, for example, Harsh *et al.*, [6]).

In this work we study, via measurements and analysis, the deformation behavior of a series of square and circular gold–polysilicon plate microstructures fabricated by the Multi-User MEMS Process (MUMPS) of Cronos (Koester *et al.*, [21]) and subjected to uniform temperature changes which generate internal stresses and deformation via thermal expansion mismatch of the gold and polysilicon. We observe linear and geometrically nonlinear deformations, as well bifurcations in the equilibrium deformed shapes. The nonlinear deformation and bifurcations depend strongly on the size of the plate. We interpret the measurements in terms of both a constant curvature analysis and detailed finite element analyses that remove this restriction. Finally, the results are discussed in the context of some MEMS applications. Guidelines are presented in the form of curvature maps as a function of microstructure geometry (plate size and shape) and temperature change for the design of plate microstructures with controlled curvature. Depending on the application, tailoring the curvature might entail minimizing it (for example, micromirrors) or maximizing it (for example, microactuators).

II. SAMPLES AND MEASUREMENTS

We designed a series of square and circular gold–polysilicon plate microstructures and fabricated them using the MUMPS surface micromachining process. The square and circular samples were fabricated using MUMPS 31 and 36, respectively. In the series of microstructures, the polysilicon layer (POLY2 in the MUMPS process) was fully covered by the gold layer. We varied the characteristic dimension l (square plate length or circular plate diameter) to include $l = 150 \mu\text{m}$, $200 \mu\text{m}$, $250 \mu\text{m}$, and $300 \mu\text{m}$, keeping the thickness of the gold and polysilicon fixed at nominal values of $0.5 \mu\text{m}$ and $1.5 \mu\text{m}$, respectively, as produced by the MUMPS process. The idea behind the design of the microstructures was to yield square and circular gold–polysilicon bilayer microstructures that rest as freely as possible. To this end, the plates were supported on the substrate by a $16\text{-}\mu\text{m}$ -diameter polysilicon post (fabricated from POLY2 through anchor2 and connected to the nitride layer). Scanning electron micrographs (SEMs) of typical plate microstructures are shown in Fig. 2.

We measured the deformation of the plate microstructures as a function of temperature change using an interferometric microscope and a custom-built thermal chamber that is covered by a quartz window to allow optical access. Full-field measurements of the out-of-plane displacement of the microstructures were made with scanning white light interferometry as the temperature was changed. The resolution of the out-of-plane displacement measurements, $w(x, y)$, is on the order of a nm as verified by making measurements on standard reference samples; the resolution of the temperature chamber is about 1°C . During tests when the temperature was being varied a 2.5X objective was used yielding a lateral spatial resolution of about

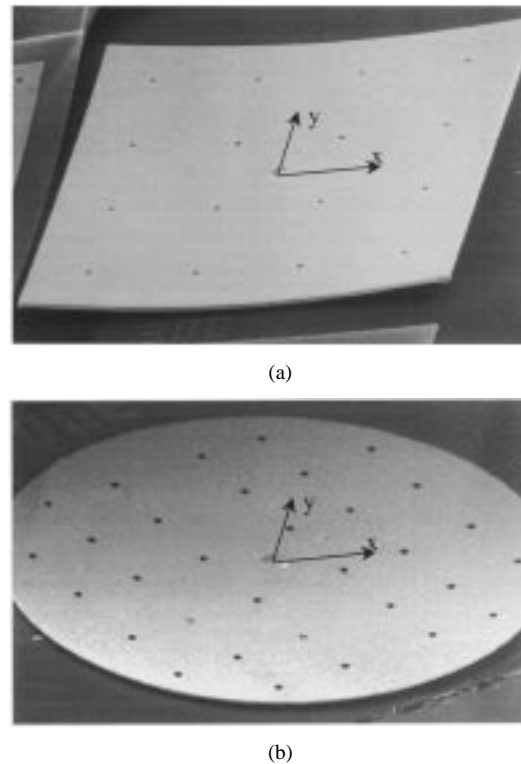


Fig. 2. SEM images of gold–polysilicon plate microstructures. The support post and etch holes are apparent and the x – y coordinate system used in subsequent measurements and analysis is identified. (a) $300 \mu\text{m} \times 300 \mu\text{m}$ square plate. (b) $300 \mu\text{m}$ diameter circular plate.

$4.7 \mu\text{m}$. At room temperature a 10X objective was also used to more accurately study the spatial variation of the deformation. In this case the lateral spatial resolution is about $1.2 \mu\text{m}$. A Michelson objective was used which has a beam-splitting element that transmits one portion of the white light beam to a reference mirror and the other to the object. The two beams reflected from the reference and the object are recombined and projected onto a charge-coupled device (CCD) video camera, to generate a signal proportional to the resultant beam intensity produced by the interference effect. These signals are then transferred into the spatial frequency domain and the surface height for each point is obtained from the complex phase as a function of the frequency. Complete details of the data reduction algorithm are given by De Groot and Deck [3] where they report subpixel/fringe accuracy of 0.1 nm (De Groot and Deck, [3]). We do not claim to have achieved such accuracy, but in our measurements we are confident that we achieve nm-scale accuracy that is more than sufficient for our purposes.

The specific test protocol is designed to ensure that the measured deformation during the temperature variations is primarily due to thermal expansion mismatch between the gold and polysilicon, and that the material behavior is thermoelastic. Specifically, the sample is heated to approximately 100°C where it is nearly flat (the deviation from a perfectly flat surface with zero curvature is always less than five percent of that observed upon subsequent cooling). The sample is held at this temperature for a time period sufficient to ensure it has reached thermal equilibrium and a stable flat shape (about 3.5 min). The sample is then slowly cooled to room temperature. The

temperature is held constant for about 3.5 min every 5 °C so that thermal equilibrium is reached, and also so that the stresses do not significantly relax due to creep of the gold and/or polysilicon (as shown elsewhere, the stresses can relax in these microstructures even at such modest temperatures (Zhang and Dunn, [29])). That this is the case is evident from the stability of the subsequent curvature measurements as described next. Full-field out-of-plane displacements $w(x, y)$ of the surface of the plate are then measured using the interferometric microscope over a circular region of about 150 μm diameter about the center of each plate. We measure only over this region, and not over the entire plate, because the slope of the displacement field outside this region is too large to be measured with the 2.5X objective. At room temperature, though, we measured $w(x, y)$ over the entire plate surface with the 10X objective. We then fit the measured $w(x, y)$ data set with a sixth-order polynomial in x and y (which was sufficient to accurately describe the displacement profile in all cases). This polynomial was then differentiated analytically to determine the approximate curvatures $\kappa_x(x, y) \approx -\partial^2 w(x, y)/\partial x^2$ and $\kappa_y(x, y) \approx -\partial^2 w(x, y)/\partial y^2$ as a function of position. Calculations of the exact curvatures, e.g., $\kappa_x = -\partial^2 w/\partial x^2 / [1 + (\partial w/\partial x)^2]^{3/2}$, were also performed and the results were found to not differ significantly from the approximate values, consistent with numerical results of Freund [14], and our own as discussed in Section III. Although we can not measure them directly, we are confident that temperature gradients in the temperature chamber contribute insignificantly to the curvature of the gold-polysilicon plate microstructures. This claim is based on measurements of curvature developed in similar size single-material polysilicon plate microstructures: they are about two to three orders of magnitude less than those developed in the gold-polysilicon plate microstructures.

III. ANALYSIS

As mentioned in the Introduction, numerous efforts have been forwarded to model the response of multilayer plate structures subjected to thermomechanical loading. Here we consider a two-layer plate with layer thicknesses t_1 and t_2 as shown in Fig. 1(a). Each layer is isotropic and characterized by the Young's modulus E_i , Poisson's ratio ν_i , and thermal expansion coefficient α_i ($i = 1, 2$). In the application to follow, we take layer 1 to be gold and layer 2 to be polysilicon. We consider two plate shapes: circular, with diameter D , and square with side length L . The plate is subject to a uniform temperature change ΔT . In order to compute the deformed shape when the plate is subject to a temperature change we use the approach of Hyer (1984) as applied by Masters and Salamon [22]. Briefly,

we assume the transverse midplane displacement is of the form $w(x, y) = d_1 x^2 + d_2 y^2$ (d_1 and d_2 are one-half the curvature in the x - and y -directions), and the in-plane displacements of the midplane are third-order polynomials in x and y , also with unknown constant coefficients to be determined. The midplane strains are then computed from the nonlinear strain-displacement relations of the von Karman plate theory

$$\begin{aligned}\varepsilon_x^o &= \frac{\partial u}{\partial x} + \frac{1}{2} \left(\frac{\partial w}{\partial x} \right)^2 \\ \varepsilon_y^o &= \frac{\partial v}{\partial y} + \frac{1}{2} \left(\frac{\partial w}{\partial y} \right)^2 \\ \gamma_{xy}^o &= \frac{\partial u}{\partial y} + \frac{\partial v}{\partial x} + \left(\frac{\partial w}{\partial x} \right) \left(\frac{\partial w}{\partial y} \right)\end{aligned}\quad (1)$$

where u , v , and w are the midplane displacements in the x , y , and z -directions, respectively. The strains at any point through the thickness are then computed using the standard kinematic relations for thin plates, and the stresses are computed from the strains using the conventional linear thermoelastic constitutive relations for each layer. The potential energy density of each layer is computed from the stress and strain in each layer, and the total potential energy of the plate is computed by integrating the potential energy density over the volume of the plate. This yields an expression for the potential energy of the plate in terms of the unknown coefficients d_i , which are determined by minimizing the total potential energy. This process yields solutions for all three regions of the deformation response of Fig. 1. Complete details regarding this analysis can be found in these references; here we present only the pertinent results in what we hope is an accessible form. When the displacements are small, the curvature $\kappa = \kappa_x = \kappa_y$ and midplane strain $\varepsilon^o = \varepsilon_x^o = \varepsilon_y^o$ depend linearly on the thermal expansion mismatch strain ($\Delta\alpha\Delta T$ where $\Delta\alpha = \alpha_2 - \alpha_1$) and can be expressed as shown in (2)–(3) at the bottom of the page where $h = t_1/t_2$ and $m = M_1/M_2$, where $M_i = E_i/(1 - \nu_i)$ ($i = 1, 2$). These results agree with those obtained by Finot and Suresh [8] and Freund *et al.*, [13] and are independent of the plate size and shape (square or circular). Note that in general both κ and ε^o are necessary to compute the stresses in the layers. An important application of these results is the *thin-film limit* where $t_1 \ll t_2$. Expanding (2) in powers of h and retaining only the lowest order term recovers Stoney's [28] well-known result which is the term outside the brackets. Many recent papers have discussed *corrections* to Stoney's result to increase the region of validity in terms of layer thicknesses and modulus mismatch. We emphasize, though, that (2) is valid for arbitrary layer thicknesses and modulus mismatch, and is quite simple to use itself. In the thin film

$$\kappa = \frac{6\Delta\alpha\Delta T}{t_2} hm \left[\frac{1+h}{1+2hm(2+3h+2h^2)+h^4m^2} \right] \quad (2)$$

$$\varepsilon^o = \frac{[\alpha_1 mh(1+3h+3h^2+mh^3) + \alpha_2(1+mh(3+3h+h^2))] \Delta T}{1+2hm(2+3h+2h^2)+h^4m^2} \quad (3)$$

limit, (3) reduces to $\alpha_2 \Delta T$. Finot and Suresh [8] and Freund [14], among others, discuss the limitations of the thin-film simplification of (2) and (3).

An important quantity for many applications where control of the deformation is important is the maximum deflection η between two points on the plate. Retaining the assumption of constant curvature, this can be expressed as

$$\eta = \frac{\kappa l^2}{8} \quad (4)$$

where again $l = L, D$ for square and circular plates, respectively. Note that for the square plate this represents the deflection between the plate center and a point on the edge along either x or $y = 0$. We emphasize that this simple result is based on the assumption of uniform curvature; the appropriateness of this assumption will be taken up in detail subsequently.

In the nonlinear, but symmetric deformation regime, the relationship between both the curvature and midplane strain and the thermal expansion mismatch is too complex to present here. This is also the case in the nonlinear regime after bifurcation. An important difference between the linear and nonlinear response, though, is that the nonlinear response depends on the plate size. The critical curvature at which bifurcation occurs, though, can be obtained explicitly and is given by

$$\kappa_{cr}^s = \frac{12\sqrt{2}}{L^2} \sqrt{\frac{6 + \frac{A_{12}}{A_{11}}}{1 + \frac{A_{12}}{A_{11}}} \frac{\sqrt{A_{66}D_{66} - B_{66}^2}}{A_{66}}} \quad (5)$$

for a square plate, and

$$\kappa_{cr}^c = \frac{32\sqrt{3}}{D^2} \sqrt{\frac{1}{1 + \frac{A_{12}}{A_{11}}} \frac{\sqrt{A_{66}D_{66} - B_{66}^2}}{A_{66}}} \quad (6)$$

for a circular plate. In (5) and (6) we have introduced the well-known composite moduli A_{ij} , B_{ij} , and D_{ij} (see, for example, Jones [19]). These are functions of the elastic moduli of the layers, the layer thicknesses, and the geometrical arrangement of the layers, and are defined and given explicitly in the Appendix. The results for the square plate agree with those of Masters and Salamon [22], [23]. In the simplified case where there is no elastic mismatch between the layers and the elastic response can be expressed in terms of the Young's modulus E and Poisson's ratio ν , (5), and (6) reduce to

$$\kappa_{cr}^i = Y^i \frac{t}{l^2} \quad (7)$$

where $t = t_1 + t_2$, $i = c, s$ for the circular and square plates respectively, and:

$$Y^c = \frac{16}{\sqrt{1+\nu}}, \quad Y^s = 2\sqrt{6} \sqrt{\frac{6+\nu}{1+\nu}}. \quad (8)$$

Equations (7) and (8) agree with the results of Finot and Suresh [8] and Freund *et al.* [13], and Freund [14]. For the material parameters of polysilicon and gold, (5) and (6) predict that a square plate will bifurcate at a smaller curvature than the circular one with $D = L$. Although we have focused on the critical curvature for bifurcation, we note that for a plate with no elastic

mismatch, the critical condition can be expressed in terms of a critical maximum deflection as $\Delta_{cr} = Y^i t/8$ (see for example, Finot and Suresh, [8]).

While the assumed displacement field used in the Ritz procedure could be modified to incorporate the dependence of curvature on position, perhaps the simplest approach to tackle these more general problems is to use the finite element method to solve the geometrically nonlinear equations over an arbitrary spatial domain. This is also the most viable approach for complicated geometries. We used this approach with the ABAQUS finite element code and used composite shell elements to approximate the thin-plate kinematics of the Kirchoff theory. Geometric nonlinearity is modeled using the well-known von Karman theory for thin plates with large deflections. Both materials are modeled as linear elastic with isotropic material properties. Input parameters to the finite element calculations are $E_2 = 163$ GPa, $\nu_2 = 0.22$ (in line with measurements of Sharpe *et al.* [25]), $E_1 = 78$ GPa, $\nu_1 = 0.42$ (King, [20]). The thermal expansion coefficients of the materials were assumed to vary linearly with temperature and values at 100(24) $^\circ$ C used are $\alpha_2 = 3.1 (2.6) \times 10^{-6}/^\circ$ C, and $\alpha_1 = 14.6 (14.2) \times 10^{-6}/^\circ$ C (King, [20]). Although some uncertainty exists in the values of these material properties for the gold and polysilicon films, we think that these values are accurate enough for the purpose of modeling the observed phenomena. Young's modulus and Poisson's ratio of the polysilicon are in line with many measurements over many MUMPS runs (Sharpe, [26]), and agree adequately with bulk polycrystal averages of single crystal elastic constants. Typical finite element meshes for the plate microstructures contained elements with a characteristic dimension of about 12.5 μ m, a size that was chosen after a convergence study with mesh size. Calculations were carried incorporating the support post and it was found to be insignificant on the resulting displacements, curvatures, and stresses except in a region very near the post. If one carries out calculations as just described, the linear and geometrically nonlinear response of the plate can be computed, but the bifurcations, and the subsequent post-bifurcation behavior, cannot because of the perfect symmetry present in the geometry and material behavior. In order to model the bifurcations, one can seed an imperfection of some sort into the model. We did this in two ways, with the hope of identifying the likely actual imperfections that contribute to the observed behavior. First, we introduced a slight thermal expansion mismatch anisotropy into the model by assuming the thermal expansion coefficient of the gold is orthotropic. Specifically, we defined the in-plane thermal expansion coefficients to be $\alpha_x = \alpha_1$ and $\alpha_y = \alpha_1 + \delta\alpha_1$, where $\delta\alpha_1$ was taken to be 0.01% of α_1 .¹ With this slight perturbation, the prebifurcation response

¹Since gold and silicon are cubic, crystallographic texture would not be expected to result in orthotropy in thermal expansion, a second-rank tensorial quantity. However, processing imperfections that lead to voids, defects, etc., could potentially lead to slight anisotropy. At present, it is probably not possible to measure thermal expansion and elastic properties on thin film samples to this accuracy, so definitive confirmation of this supposition is lacking. We note though that the stress developed upon a uniform temperature change depend on the thermal expansion and elastic moduli. The latter, being fourth-rank tensors, would exhibit orthotropy in the presence of general crystallographic texture.

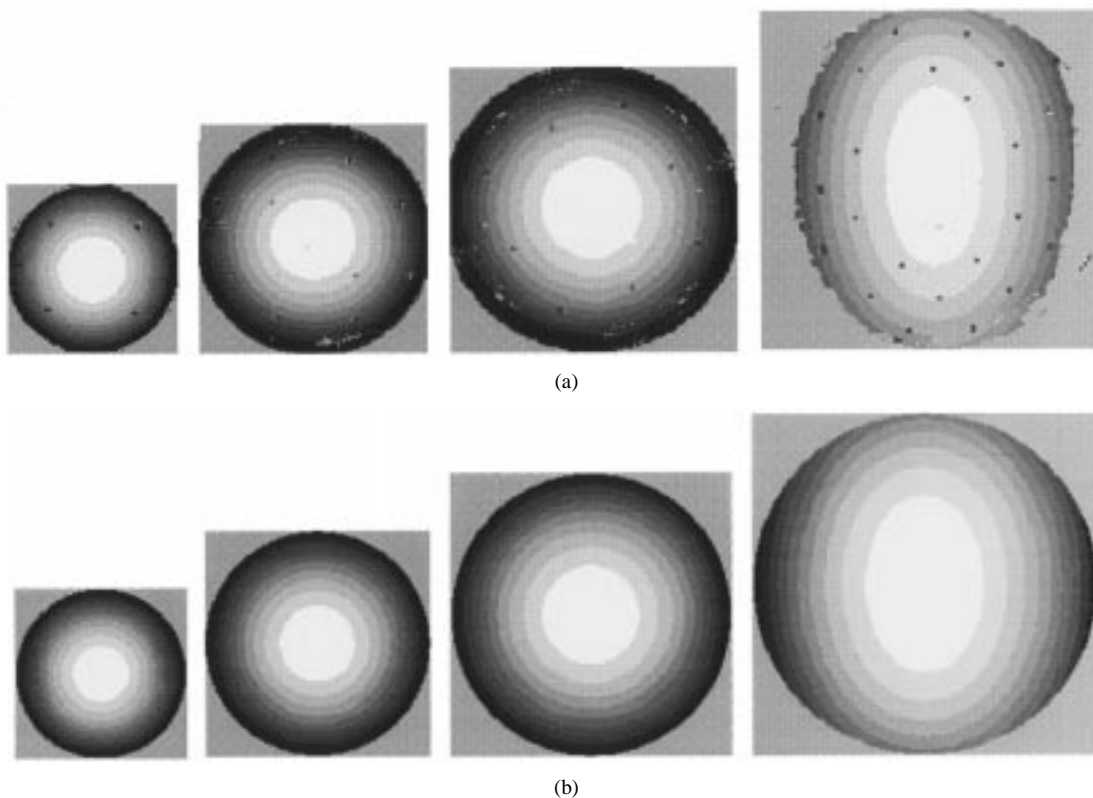


Fig. 3. Contour plots of the (a) measured, and (b) predicted transverse displacements $w(x, y)$ at room temperature for the four gold-polysilicon circular plates: $D = 150, 200, 250,$ and $300 \mu\text{m}$ from left to right. Each contour band represents a displacement of $0.13, 0.22, 0.29,$ and $0.48 \mu\text{m}$ for the $D = 150, 200, 250,$ and $300 \mu\text{m}$ plates, respectively.

was indistinguishable from that with the isotropic thermal expansion. The second approach to seed the imperfection was only used for the square plates; we defined one side of the plate to be slightly larger than the other, i.e., the plate has dimensions $L \times (L + \Delta L)$. As discussed by Freund [14], details of the bifurcation, especially its sharpness, are strongly influenced by small changes in the imperfection. We discuss this later in light of both our measurements and predictions. Calculations were carried out for the loading situation of an applied uniform temperature change consistent with that experienced in the measurements.

IV. RESULTS AND DISCUSSION

Figs. 3 and 4 show contour plots of the measured and predicted displacement field $w(x, y)$ at room temperature for the circular and square plates of all four plate sizes. Due to the thermal expansion mismatch between the polysilicon and gold, the $l = 150 \mu\text{m}$ samples deform in a spherically symmetric manner; contours of constant transverse displacement $w(x, y)$ are nearly circles. This is also the case as the size increases to $l = 200$ and $250 \mu\text{m}$, although the displacements increase as the plate size increases. At $l = 300 \mu\text{m}$, though, the transverse displacement contours are not circular, but elliptical, indicating that the deformation is no longer spherically symmetric. It is apparent that when subjected to the same temperature change, both the magnitude and deformation mode of the different size plates depend on the plate size. As the in-plane dimension of the plate increases with the thickness held constant, the deformation

mode changes from one of spherical symmetry to one more like cylindrical symmetry. Both the measured and predicted $w(x, y)$ contours show this same behavior and the agreement between them is quite good. The deformation behavior for all plate sizes is similar for both the square and circular plates, particularly over the inner regions of the plate away from the edges. As we will describe later, proper normalization of the curvature and temperature change yields the functional form of this size dependence before bifurcation.

In Figs. 5 and 6, we plot the average curvature in the x - and y -directions as a function of the magnitude of the temperature change during cooling. The temperature change is actually negative according to our convention but its magnitude is plotted for convenience throughout the paper. Note that the results would be the same, but with the sign of the curvature changed, if a temperature change resulting in heating were used as long as no material nonlinearity is present. In Figs. 5 and 6 measurements are shown with symbols (the lines connecting them are used simply to aid viewing), and the finite element predictions are shown with solid lines. In these plots, the average curvatures are determined from the measured and computed $w(x, y)$ by averaging $\kappa_x = -\partial^2 w(x, 0)/\partial x^2$ and $\kappa_y = -\partial^2 w(0, y)/\partial y^2$ along the paths $y = 0$ and $x = 0$, respectively, over a region of $150 \mu\text{m}$ diameter from the center of the plate. Again, this is the extent of the region that is experimentally accessible. The x - and y -directions are taken to be aligned with the principal curvatures after bifurcation. Before bifurcation, the response is spherically symmetric and so the x - and y -directions are arbitrary and indistinguishable. The use of the average curvature as a measure

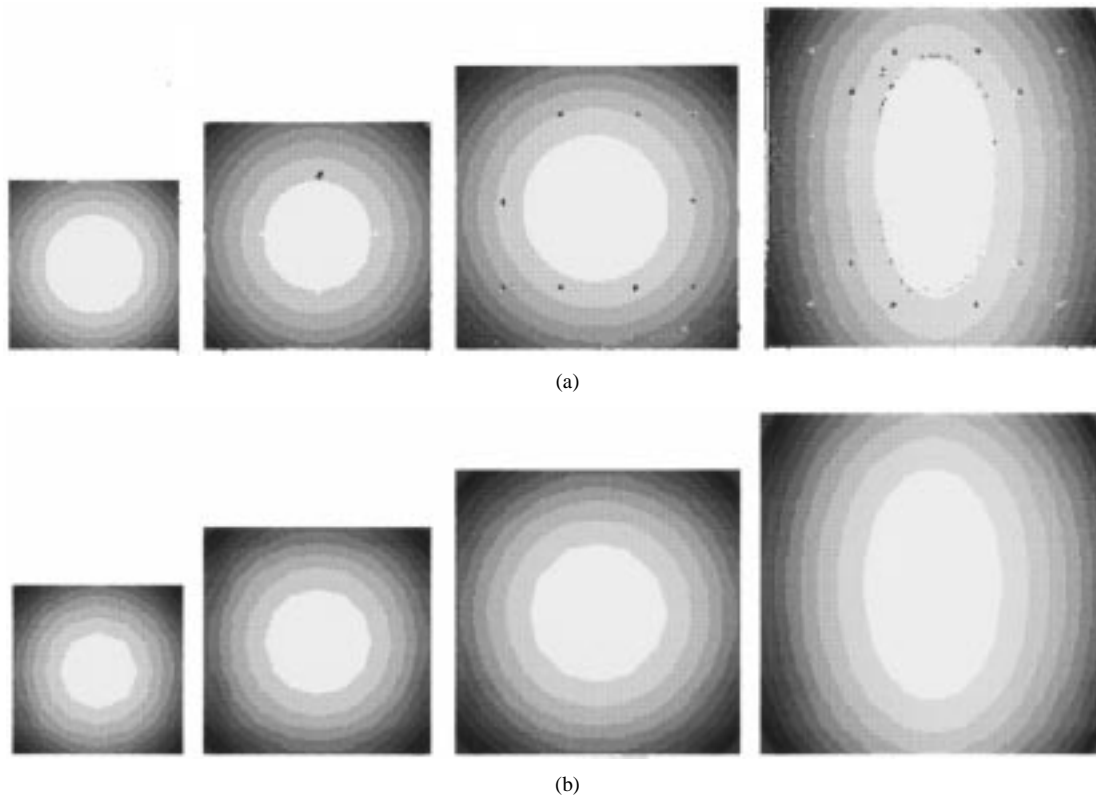


Fig. 4. Contour plots of the (a) measured, and (b) predicted transverse displacements $w(x, y)$ at room temperature for the four gold-polysilicon square plates: $L = 150, 200, 250,$ and $300 \mu\text{m}$ from left to right. Each contour band represents a displacement of $0.23, 0.35, 0.45,$ and $0.6 \mu\text{m}$ for the $L = 150, 200, 250,$ and $300 \mu\text{m}$ plates, respectively.

of the plate deformation seems appropriate if the curvature is, or is close to, spatially uniform. This aspect will be taken up to some degree later. The measurements and predictions in Figs. 5 and 6 show the three regimes of deformation as discussed in the Introduction. It is apparent from both the measurements and predictions that in regime *I*, the curvature-temperature response is independent of plate size and shape. In regime *II*, though, there is a strong dependence on plate size. Although only one set of data exists in regime *III*, calculations and measurements that are not shown demonstrate a dependence on plate size and shape. Figs. 5 and 6 show good agreement between the measurements and predictions in all three deformation regimes. The major discrepancy is the sharpness of the bifurcation for the $l = 300 \mu\text{m}$ plates; it is quite sharp in the predictions but much more gradual in the measurements. There is of course a related discrepancy in the temperature change at which the bifurcation occurs. To understand this we remind that the source of the bifurcation is an *imperfection* of some sort that breaks the ideal symmetry; we will take this up in more detail in the following.

Following Freund *et al.* [13] and Freund [14], we introduce the nondimensional curvature K and temperature change (mismatch strain) S

$$K = \frac{\kappa \ell^2}{16t_2}$$

$$S = \frac{3\Delta\alpha\Delta T\ell^2 t_1 M_1}{8t_2^3 M_2}$$

In these expressions, $\ell = D, L$ for the circular and square plates, respectively. The data of Figs. 5 and 6, before bifurcation, are

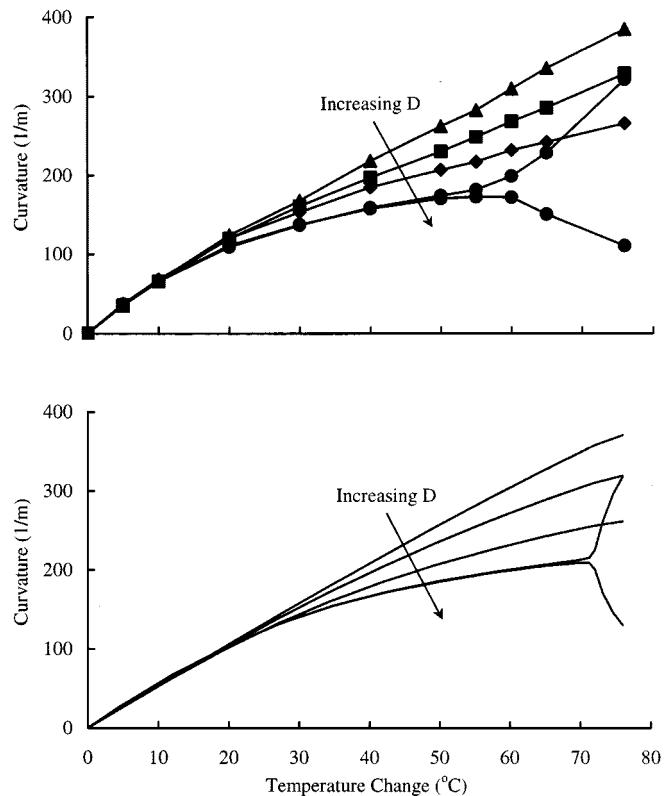


Fig. 5. Average measured (top) and predicted (bottom) curvature as a function of temperature change upon cooling from $100 \text{ }^\circ\text{C}$ to room temperature. The curves from top to bottom are for the $D = 150, 200, 250,$ and $300 \mu\text{m}$ microstructures, respectively.

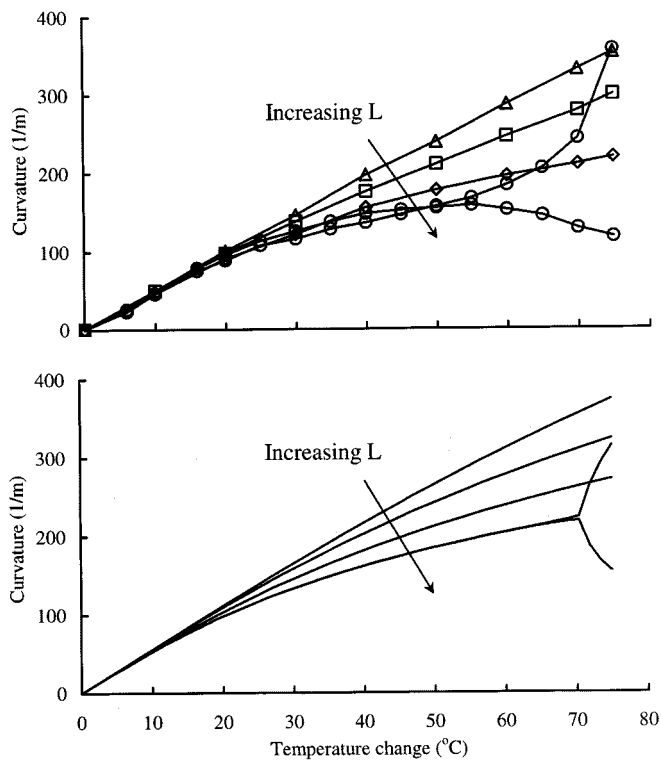


Fig. 6. Average measured (top) and predicted (bottom) curvature as a function of temperature change upon cooling from 100 °C to room temperature. The curves from top to bottom are for the $L = 150, 200, 250,$ and $300\mu\text{m}$ microstructures, respectively.

plotted in terms of these nondimensionalized variables in Fig. 7. The four curves collapse to a single curve and the plate size effect in this regime is described by the nondimensionalization. We emphasize, though, that this is in part because the average curvature is computed over a region of $150\mu\text{m}$ diameter, and the curvature is relatively uniform over this region. In agreement with Freund's results, the geometric nonlinear effects initiate at a normalized temperature change (mismatch strain) of about $S = 0.3$. Interestingly, predictions for both the circular and square plates are indistinguishable, but the measurements differ slightly, particularly at larger values of S . Here the results for the circular microstructures are slightly above those for the square microstructures. The reason for this is unclear, but it is perhaps due to slight differences in properties between the two fabrication runs to produce the two sets of samples. Nevertheless, the agreement between the measurements and predictions is quite good.

In Figs. 8 and 9 we explore the connection between the thermomechanical loading (the temperature change), the geometry (plate size), and the boundaries between the three deformation regimes for the gold-polysilicon plate microstructures. Fig. 8 shows the temperature change necessary to initiate nonlinear effects (the transition between regions *I* and *II*) as a function of polysilicon thickness when the gold film thickness is kept constant at $0.5\mu\text{m}$. Fig. 9 shows similar results for the onset of bifurcation (the transition between regions *II* and *III*). For simplicity, the calculations leading to these results were carried out using the analytical model previously described. Limited results obtained from finite element calculations are in reasonable

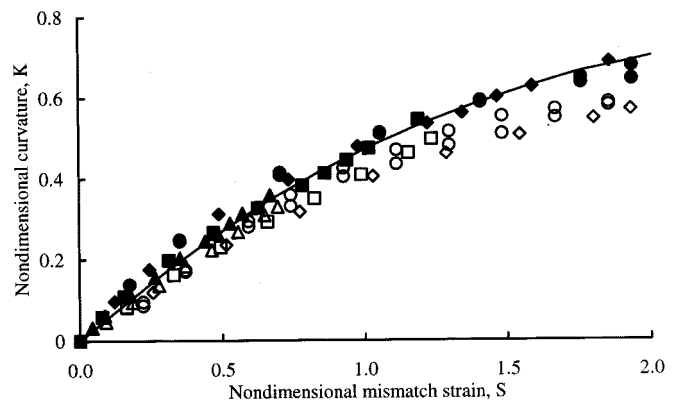


Fig. 7. Nondimensional average curvature as a function of temperature change for the linear and nonlinear regimes. Measurements (symbols: filled for circular plates, and open for square plates) and predictions (solid line for both circular and square plates) are shown. Both open and close symbol shapes denote the same plate sizes as in Figs. 5 and 6, i.e., $l = 150\mu\text{m}$ (triangles), $l = 200\mu\text{m}$ (squares), $l = 250\mu\text{m}$ (diamonds), and $l = 300\mu\text{m}$ (circles).

agreement with these, particularly qualitatively (the differences can be seen to some degree in Fig. 14, although that is not the primary intent of that figure). In each figure, contours for constant polysilicon layer thicknesses are shown. Of particular note are $t = 1.5\mu\text{m}$ and $t = 3.5\mu\text{m}$. These thicknesses correspond to plates fabricated from the POLY2 and POLY2 + POLY1 layers in the MUMPS process. The curve $t = 4.5\mu\text{m}$ corresponds approximately to the case of a plate fabricated from the MUMPS POLY2 + OXIDE + POLY1 layers, i.e., a structure fabricated with a trapped oxide layer (Cowan *et al.*, [1]). It is approximate because the elastic moduli of the oxide differ from that of polysilicon. Also notable are the curves for $t = 8.5\mu\text{m}$. These are applicable to a polysilicon process that is capable of depositing more structural layers, such as the Sandia SUMMIT process (see for example, Sniegowski and de Boer, [27]). Figs. 8 and 9 show the strong influence of the plate length/thickness ratio on the development of geometrically nonlinear deformation and bifurcation.

In Fig. 10, we explore the effect of possible imperfections that may trigger the bifurcation in the deformation behavior. In order to simplify the interpretation of the results and identify basic phenomenological features, the calculations in Fig. 10 were carried out with constant room temperature material properties. This slightly alters the exact magnitudes of calculated quantities, but does not affect the conclusions drawn. This can be seen quantitatively by comparing the results here with those in Fig. 6 which incorporate temperature-dependent material properties. First, in Fig. 10(a) we alter the thermal expansion mismatch by increasing the thermal expansion coefficient of the gold $\alpha_x = \alpha_1$ and $\alpha_y = \alpha_1 + \delta\alpha$, while keeping $\delta\alpha$ fixed. This increases the mismatch strain $\Delta\alpha\Delta T$. Note that the same effect could be generated by decreasing the thermal expansion of the polysilicon while keeping that of the gold constant since the thermal expansion mismatch drives the deformation. Fig. 10(a) shows that increasing the mismatch strain by about 8.5% decreases the temperature at which bifurcation occurs by about 5°C , but at the resolution of the plot it does not significantly affect the linear and nonlinear portions of the temperature-curvature response. Of course these results are for the particular

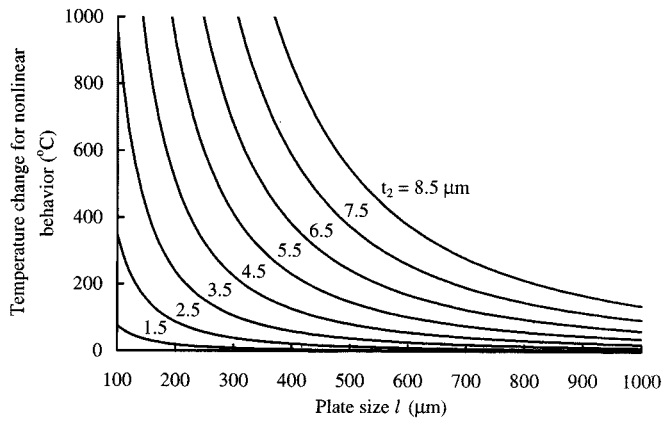


Fig. 8. Temperature change required for the initiation of nonlinear geometry effects as a function of plate size and the thickness of polysilicon for the gold-polysilicon microstructures.

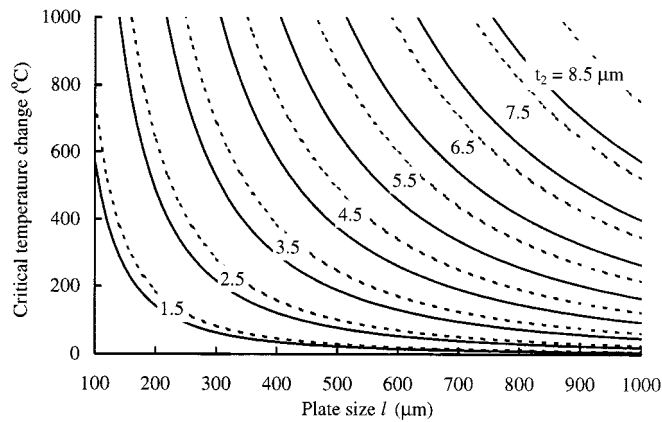
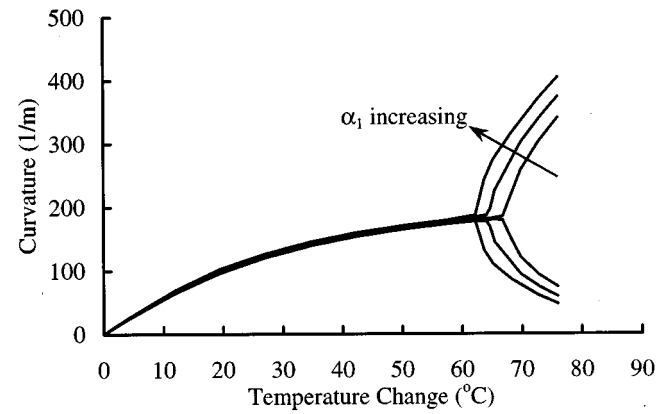


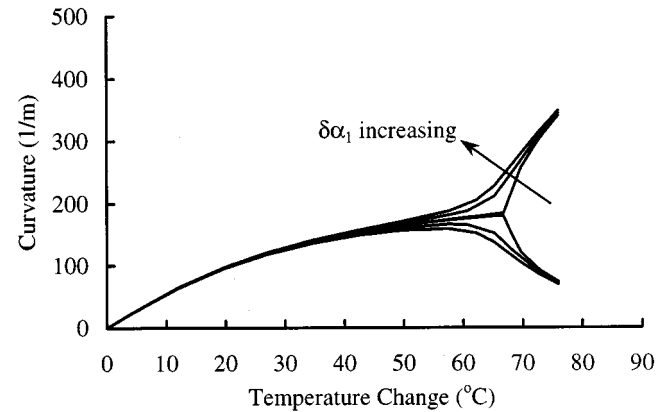
Fig. 9. Critical temperature change for bifurcation as a function of plate size and the thickness of polysilicon for the square (solid lines) and circular (dashed lines) gold-polysilicon microstructures.

material system and geometry considered. This 8.5% difference in the mismatch strain is probably not an unrealistic estimate of the uncertainty of the actual mismatch strain. Looking at these results in light of the measurements, it seems that the uncertainty in knowledge of the mismatch strain can not explain the discrepancy between the observed and predicted deformation. This is because it is not adequate to predict the observed difference between the measured and predicted temperature at which bifurcation occurs, and because it does not resolve the difference in the sharpness of the bifurcation between measurements and predictions.

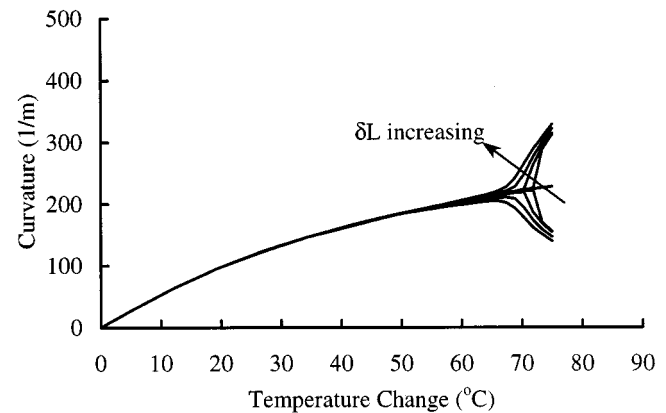
In Fig. 10(b), we study the effect of slight anisotropy in the mismatch strain by increasing the thermal expansion anisotropy of the gold, $\delta\alpha_1$. The principal result of this is a gradual beginning of the bifurcation, from the sharp result with $\delta\alpha_1 = 0.004$, as $\delta\alpha_1$ is increased. To the resolution of the plot, no significant effect is observed in the linear and nonlinear regimes prior to bifurcation. Interestingly, anisotropy in α_1 of less than one percent leads to a decrease in temperature change at the beginning of the bifurcation of about 15–20 °C. The latter is in line with the discrepancy between measurements and predictions, and the former is probably not an unreasonable degree of anisotropy as discussed previously. We note, though, that because of the decrease in the sharpness of the bifurcation it is difficult to describe



(a)



(b)



(c)

Fig. 10. Effects of an initial imperfection on the bifurcation for the $L = 300 \mu\text{m}$ plate: (a) effect of α_1 : $\alpha_1 = 14.5, 15,$ and $15.5 \times 10^{-6}/^\circ\text{C}$; (b) effect of $\delta\alpha_1$: $\delta\alpha_1 = 0.004, 0.1,$ and $0.2 \times 10^{-6}/^\circ\text{C}$; and (c) effect of δL : $\delta L = 0.05, 0.1, 0.5, 3,$ and $6 \mu\text{m}$.

precisely the temperature change at which the bifurcation starts. In Fig. 10(c), we study the effect of imperfection in the structural geometry, specifically, the side length of the square plate. Like the thermal expansion anisotropy, increased small anisotropy in the plate side length δL leads primarily to a gradual beginning of the bifurcation. Here $\delta L = 6 \mu\text{m}$ leads to only about a 7–10 °C decrease in the beginning of the bifurcation. The latter is less than that observed in the measurements and the former is much larger than the δL measured which is about one μm at most. As a result, anisotropy in the geometry is probably not the primary imperfection that actually contributes to the gradual bifurcation.

These results, along with similar ones reported by Freund *et al.*[13] and Freund [14], show that the details of the bifurcation are strongly influenced by slight perturbations of the imperfection. This sensitivity probably precludes a sharp bifurcation in practice. Although we focused on the possible roles of $\delta\alpha_1$ and δL , other imperfections such as other slight variations in the geometry, nonuniformities in the layer thicknesses due to deposition imperfections, the etch holes, and anisotropy and/or heterogeneity in other material properties also can play a role in the exact bifurcation details. In summary, the bifurcation details are a strong function of the details of the imperfections and probably represent an aggregate effect of all of these. As a result, it is prohibitively difficult to predict the bifurcation details. We note, though, that if it is desired to make the bifurcation occur in a particular direction one can incorporate an imperfection into the microstructure design, for example, anisotropy in the length, that overwhelms all other sources of imperfections that may not be able to be accurately controlled.

In the analytical treatments discussed previously it is assumed that the curvature is spatially uniform. The power of the finite element calculations is that this requirement is relaxed and the spatial variation of the curvature can be studied. Our full-field measurement capability allows us to study this experimentally as well. We take up this line of inquiry in Figs. 11 and 12 where predicted and measured curvatures $\kappa_x(x, 0)$ and $\kappa_y(0, y)$ are plotted as a function of temperature change for four discrete positions along the x -axis ($y = 0$) and y -axis ($x = 0$), respectively, for the $l = 300 \mu\text{m}$ microstructures. In the linear regime, the curves are indistinguishable implying that the curvature is essentially uniform across the plate. In the nonlinear regime, though, the curvature varies appreciably with position, increasing by about a factor of two from the center to the periphery of the plate. As with the average curvature, good agreement also exists between measurements and predictions here, with the most significant discrepancy being the details of the bifurcation as discussed previously. Although not shown, additional calculations have shown that the spatial nonuniformity of the curvature increases as the plate size increases. The spatial variation of the curvature raises concern regarding the suitability of an analysis based on constant curvature. As mentioned previously, such an analysis may be adequate to describe the general deformation behavior, but not finer details.

While to this point we have primarily focused on curvature, in Fig. 13 we show the computed dependence of the midplane strain on the temperature change at five discrete positions on a square plate with $L = 300 \mu\text{m}$. Although not as prominent, the three deformation regimes described in the context of the curvature versus temperature change ($\kappa - \Delta T$) response are apparent in the $\varepsilon^o - \Delta T$ response. In regimes I and II, $\varepsilon_x^o = \varepsilon_y^o = \varepsilon^o$, while after the bifurcation (regime III) $\varepsilon_x^o \neq \varepsilon_y^o$ as the deformation is no longer symmetric. The midplane strains vary nearly linearly with temperature throughout the deformation; the nonlinearity in region II is slight. Additionally, the midplane strains do not vary significantly with position, especially when compared to the curvature variations of Figs. 11 and 12. This has important implications for strain measurements using X-ray or neutron diffraction as it suggests fairly large in-plane dimensions could be used for the sampling. Interest-

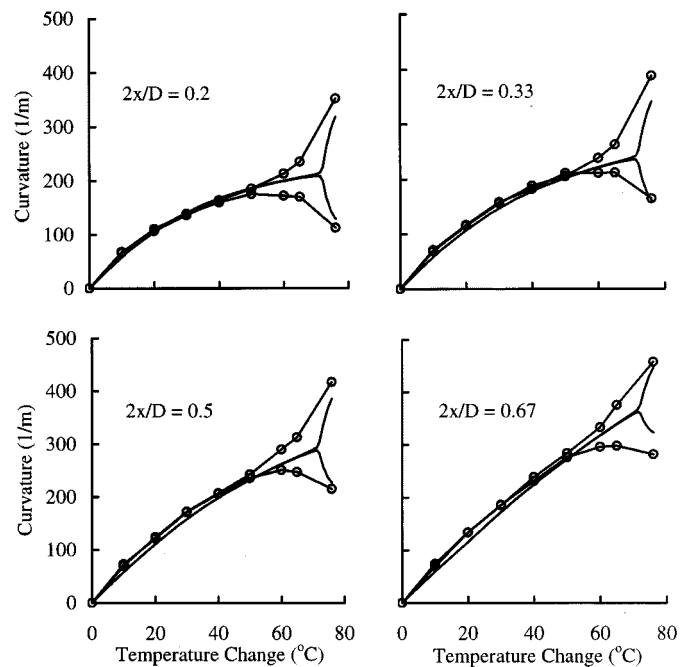


Fig. 11. Pointwise curvature as a function of temperature change for the $D = 300 \mu\text{m}$ microstructure at four locations, $2x/D = 2y/D$. Solid lines are predictions and the open circles are measurements which are connected by lines to aid viewing.

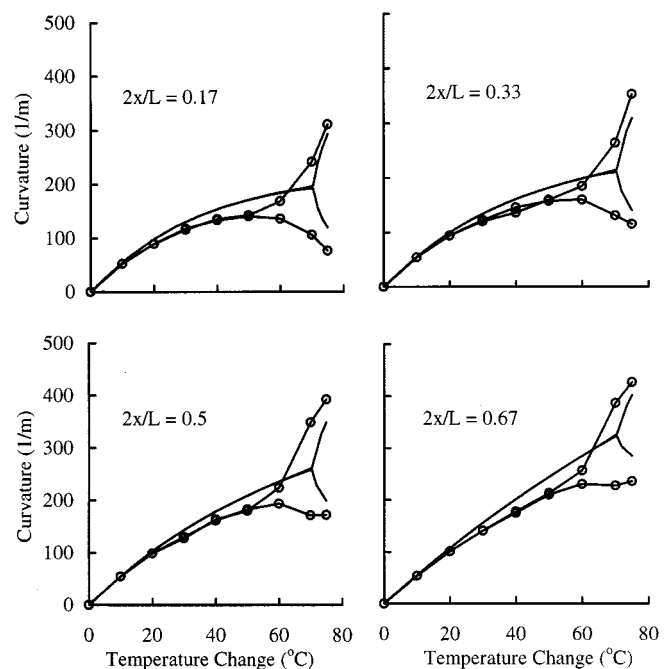


Fig. 12. Pointwise curvature as a function of temperature change for the $L = 300 \mu\text{m}$ microstructure at four locations, $2x/L = 2y/L$. Solid lines are predictions and the open circles are measurements which are connected by lines to aid viewing.

ingly, unlike the curvature variation with position, the midplane strains do not vary monotonically with position from the center to the periphery of the plate. This is perhaps difficult to see from Fig. 13(a), so in Fig. 13(b), we show the two contributions to ε_x^o ($(\partial w^o / \partial x)$ and $1/2(\partial w^o / \partial x)^2$), along with ε_x^o itself, as a function of x plotted along $y = 0$ when the plate is subjected to

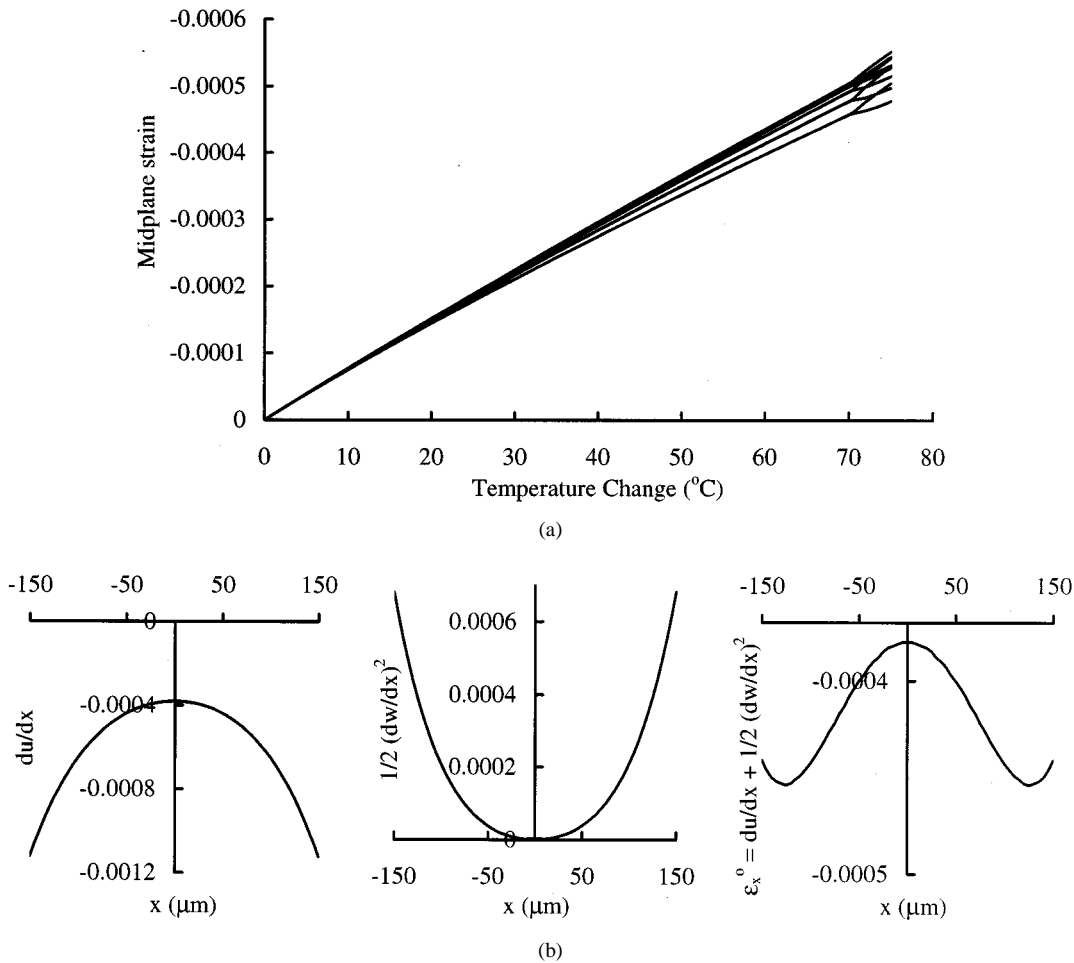


Fig. 13. (a) Pointwise midplane strain ε_x^0 (and ε_y^0) at five locations $2x/L$ (and $2y/L$) as a function of temperature change for the $L = 300 \mu\text{m}$ microstructure. Curves before bifurcation correspond to $2x(2y)/L = 0.67, 0.83, 0.5, 0.33,$ and 1 from top to bottom; (b) Midplane strain for the $L = 300 \mu\text{m}$ microstructure and its components du/dx , and $(1/2)(dw/dx)^2$ along $y = 0$ for $\Delta T = -76 \text{ }^\circ\text{C}$.

$\Delta T = -76 \text{ }^\circ\text{C}$. This illustrates the role played by the geometrical nonlinearity; the variation of the $(1/2)(\partial w/\partial x)^2$ term largely cancels out the variation of the $(\partial u^0/\partial x)$ term.

In Fig. 14 we plot the critical average curvature at which the bifurcation in the equilibrium shape occurs as a function of the plate size L . Although not shown, similar behavior results for the circular plate with diameter D . Four results are shown: i) an analytical prediction from the constant curvature calculation as given by (5); ii) predictions from the simplification where there is no elastic mismatch between the layers, (7); iii) finite element predictions; and iv) the measurement for the $L = 300 \mu\text{m}$ sample. Despite the fact that the constant curvature approximation becomes questionable for larger plate sizes, (5) is a good approximation as seen by the agreement with the finite element calculations, at least for the elastic mismatch and plate sizes considered here. In fact, the simplified result of (7) for no elastic mismatch is in reasonable agreement with the finite element and the complete analytical results. Even better agreement would be expected for practical situations where the elastic mismatch were less such as silicon dioxide/gold and silicon dioxide/aluminum multilayers. The finite element calculations are shown with error bars. These error bars show the range of critical curvature (actually critical temperature change as shown in the figure)

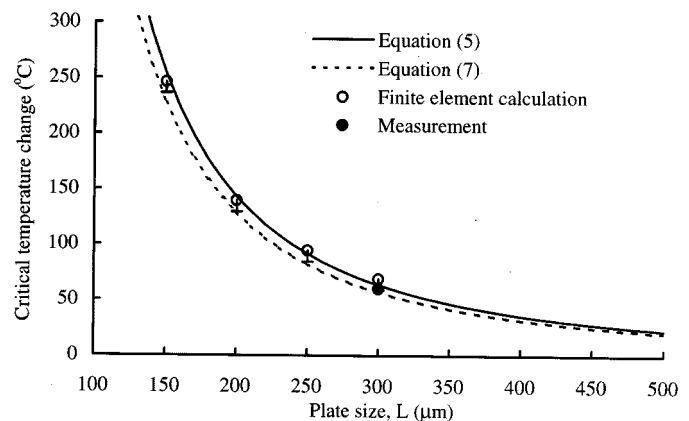


Fig. 14. Critical temperature change for bifurcation as a function of square plate size for the gold-polysilicon microstructures. The error bars on the finite element calculations represent the difference in the critical temperature change that results from a one percent change in the anisotropy of the mismatch strain (as discussed with regard to Fig. 10).

that results from a one percent change in the anisotropy of the mismatch strain (as discussed with regard to Fig. 10). Unfortunately we only have a single measurement, but it is accurately described by both the analytical and finite element results.

V. CONCLUSION

We studied the deformation response of polysilicon/gold square and circular plate microstructures subjected to uniform temperature changes. Consistent with previous observations, we observed three regimes of deformation in terms of the average curvature-temperature response: *I* linear thermoelastic response, *II* geometric nonlinear response, and *III* bifurcations in the deformation behavior. These phenomena, particular regimes *II* and *III*, can be detrimental when dimensional stability is a requirement, or can be beneficial for actuator applications. In all three regimes, we found good agreement between measurements and predictions, the latter based on both an analytical calculation assuming a constant curvature deformation mode, and finite element calculations that removed this restriction. While simple analyses assuming a constant curvature deformation mode are perhaps sufficient for simple shapes (e.g., relatively simple blanketed or thin line patterns), the finite element approach is better suited for arbitrary geometry with spatially varying curvature. The most significant discrepancies between the measurements and predictions occurred in the details of the bifurcations, but we showed that these are unlikely to be accurately modeled without detailed information regarding the imperfection that initially triggers the bifurcation. When geometric nonlinearity occurs, the average curvature depends on the in-plane dimensions of the plate, and the curvature can vary significantly over the in-plane dimensions. The average curvature may thus be insufficient to adequately describe the deformation state of the microstructure. The spatially nonuniform curvature, and thus stresses, makes the use of common average curvature measurements to determine film stress, via the Stoney formula, questionable; interpretation of such measurements must be made with care. Finally, although our focus has been on deformation, we note that significant differences exist with regard to the stress state due to the comparable thicknesses of the layers, but these will be discussed elsewhere.

APPENDIX

The composite moduli used in the text are defined in most standard texts on composite materials (see for example, Jones [19]), and are recorded here for completeness

$$\begin{aligned} A_{ij} &= \bar{Q}_{ij_1}(z_1 - z_0) + \bar{Q}_{ij_2}(z_2 - z_1) = \bar{Q}_{ij_1}t_1 + \bar{Q}_{ij_2}t_2 \\ B_{ij} &= \frac{1}{2} \{ \bar{Q}_{ij_1}(z_1^2 - z_0^2) + \bar{Q}_{ij_2}(z_2^2 - z_1^2) \} \\ D_{ij} &= \frac{1}{3} \{ \bar{Q}_{ij_1}(z_1^3 - z_0^3) + \bar{Q}_{ij_2}(z_2^3 - z_1^3) \} \end{aligned} \quad (A1)$$

where z_i and t_i are defined in Fig. 1(a). In terms of t_1 and t_2 :

$$z_0 = -\frac{t_1 + t_2}{2}, \quad z_1 = \frac{t_1 - t_2}{2}, \quad z_2 = \frac{t_1 + t_2}{2}. \quad (A2)$$

In (A1), the \bar{Q}_{ij_i} depend on the generally anisotropic elastic moduli of the i th layer; for isotropic materials the nonzero components reduce to,

$$\begin{aligned} \bar{Q}_{11_i} &= \bar{Q}_{22_i} = \frac{E_i}{1 - \nu_i^2}, \\ \bar{Q}_{12_i} &= \bar{Q}_{21_i} = \frac{\nu_i E_i}{1 - \nu_i^2} = \nu_i \bar{Q}_{11_i} \\ \bar{Q}_{66_i} &= G_i = \frac{\bar{Q}_{11_i} - \bar{Q}_{12_i}}{2} \end{aligned} \quad (A3)$$

where E_i , ν_i , and $G_i = E_i/(2(1 + \nu_i))$ are Young's modulus, Poisson's ratio, and the shear modulus, respectively, of the i th layer.

REFERENCES

- [1] W. D. Cowan, V. M. Bright, A. A. Elvin, and D. A. Koester, "Modeling of stress-induced curvature in surface-micromachined devices," *Proc. SPIE*, vol. 3225, pp. 56–67, 1997.
- [2] M. L. Dano and M. W. Hyer, "Thermally-induced deformation behavior of unsymmetric laminates," *Int. J. Solids Structures*, vol. 17, pp. 2101–2120, 1998.
- [3] P. De Groot and L. Deck, "Surface profiling by analysis of white-light interferograms in the special frequency domain," *J. Modern Opt.*, vol. 42, pp. 389–401, 1995.
- [4] M. L. Dunn, Y. Zhang, J. M. Roy, P. E. W. Labossiere, and V. M. Bright, "Nonlinear deformation of multilayer MEMS structures," in *Proc. MEMS Symp.*, Nashville, TN, Nov. 14–19, 1999, pp. 75–80.
- [5] K. F. Harsh, W. Zhang, V. M. Bright, and Y. C. Lee, "Flip-chip assembly for Si-based RF MEMS," in *Proc. 12th IEEE Int. Conf. Microelectromechanical Systems (MEMS '99)*, 1998, pp. 273–278.
- [6] K. F. Harsh, P. E. Kladitis, Y. Zhang, M. L. Dunn, V. M. Bright, and Y. C. Lee, "Tolerance and precision study for solder self-assembled MEMS," in *Proc. 2000 EUROPTO Int. Symp. Applied Photonics (ISAP 2000)*, 2000, pp. 273–278.
- [7] D. E. Fahnline, C. B. Masters, and N. J. Salamon, "Thin film stress from nonspherical substrate bending measurements," *J. Vac. Sci. Technol. A*, vol. 9, pp. 2483–2487, 1991.
- [8] M. Finot and S. Suresh, "Small and large deformation of thick and thin film multilayers: Effects of layer geometry, plasticity and compositional gradients," *J. Mech. Phys. Solids*, vol. 44, pp. 683–721, 1996.
- [9] M. Finot, I. A. Blech, S. Suresh, and H. Fujimoto, "Large deformation and geometric instability of substrates with thin film deposits," *J. Appl. Phys.*, vol. 81, pp. 3457–3464, 1997.
- [10] L. B. Freund, "The stress distribution and curvature of a general compositionally graded semiconductor layer," *J. Crystal Growth*, vol. 132, pp. 341–344, 1993.
- [11] —, "Some elementary connections between curvature and mismatch strain in compositionally graded thin films," *J. Mech. Phys. Solids*, vol. 44, pp. 723–736, 1996.
- [12] —, "The mechanics of a free-standing strained film/compliant substrate system," in *Thin Films: Stresses and Mechanical Properties VI*, vol. 436, Mater. Res. Soc. Proc., W. W. Gerberich, H. Gao, J. E. Sundgren, and S. P. Baker, Eds., 1997, pp. 393–404.
- [13] L. B. Freund, J. A. Floro, and E. Chason, "Extension of the stoney formula for substrate curvature to configurations with thin substrate or large deformations," *Applied Physics Letters*, vol. 74, pp. 1987–1989, 1999.
- [14] L. B. Freund, "Substrate curvature due to thin film mismatch strain in the nonlinear deformation range," *J. Mech. Phys. Solids*, vol. 48, pp. 1159–1174, 2000.
- [15] B. D. Harper and C.-P. Wu, "A geometrically nonlinear model for predicting the intrinsic film stress by the bending plate method," *Int. J. Solids Structures*, vol. 26, pp. 511–525, 1990.
- [16] M. W. Hyer, "Some observations on the cured shape of thin unsymmetric laminates," *J. Compos. Mater.*, vol. 15, pp. 175–194, 1981a.
- [17] —, "Calculation of the room-temperature shapes of unsymmetric laminates," *J. Compos. Mater.*, vol. 15, pp. 296–310, 1981b.
- [18] —, "The room-temperature shape of four-layer unsymmetric cross-ply laminates," *J. Compos. Mater.*, vol. 16, pp. 318–340, 1982.

- [19] R. M. Jones, *Mechanics of Composite Materials*: Taylor & Francis, 1999.
- [20] J. A. King, *Materials Handbook for Hybrid Microelectronics*. Los Angeles, CA: Teledyne Microelectronics, 1988.
- [21] D. A. Koester, R. Mahadevan, B. Hardy, and K. W. Markus, *MUMPS™ Design Rules*: Cronos Integrated Microsystems, A JDS Uniphase Company, 2001.
- [22] C. B. Masters and N. J. Salamon, "Geometrically nonlinear stress-deflection relations for thin film/substrate systems," *Int. J. Engng. Sci.*, vol. 31, pp. 915–925, 1993.
- [23] —, "Geometrically nonlinear stress-deflection relations for thin film/substrate systems with a finite element comparison," *J. Appl. Mech.*, vol. 61, pp. 872–878, 1994.
- [24] N. J. Salamon and C. B. Masters, "Bifurcation in isotropic thin film/substrate plates," *Int. J. Solids Structures*, vol. 32, pp. 473–481, 1995.
- [25] W. N. Sharpe, B. Yuan, and R. L. Edwards, "A new technique for measuring the mechanical properties of thin films," *Journal of Microelectromechanical Systems*, vol. 6, pp. 193–199, 1997.
- [26] W. N. Sharpe, "Mechanical Properties of MEMS Materials," in A Chapter in the CRC Handbook of MEMS, M. Gad-el-Hak, Ed., 2001, to be published.
- [27] J. J. Sniegowski and M. P. de Boer, "IC-Compatible polysilicon surface micromachining," *Annu. Rev. Mater. Sci.*, vol. 30, pp. 299–333, 2000.
- [28] G. G. Stoney, "The tension of metallic films deposited by electrolysis," *Proc. Roy. Soc. London*, vol. A82, pp. 172–175, 1909.
- [29] Y. Zhang and M. L. Dunn, "Stress relaxation of gold/polysilicon layered MEMS microstructures subjected to thermal loading," in *Proc. MEMS Symp., ASME Int. Mechanical Engineering Congress Exposition*, vol. 3, 2001, pp. 149–156.



Martin L. Dunn received the Ph.D. degree in mechanical engineering from the University of Washington in 1992.

He is an Associate Professor of Mechanical Engineering at University of Colorado at Boulder. His research interests include the micromechanical behavior (deformation and fracture) of materials and structures for MEMS applications, the micromechanics and physics of heterogeneous media, including defects, polycrystals, and composites, and the acoustic characterization of material microstructure. He has published over 70 articles in refereed journals on these subjects and has served as the Principal or Co-Principal Investigator on grants and contracts in these areas from NSF, NIST, DOE, DARPA, Sandia National Laboratories, and various companies.



(MEMS) applications.

Yanhang Zhang received the Bachelor of Science degree in engineering mechanics from Tsinghua University, China, in 1998 and the Master of Science degree in mechanical engineering from the University of Colorado at Boulder in May 2000. She is currently working towards the Ph.D. degree in mechanical engineering at University of Colorado at Boulder.

Her research interests are in design, modeling, and testing of the thermomechanical behavior of thin film microstructures for microelectromechanical systems



Victor M. Bright (S'89–M'92) received the B.S.E.E degree from the University of Colorado at Denver in 1986 and the M.S. and Ph.D. degrees from the Georgia Institute of Technology, Atlanta, in 1989 and 1992, respectively.

He is an Associate Professor of Mechanical Engineering and the Director of the MEMS R&D Laboratory, University of Colorado at Boulder. Prior to joining the University, he was an Associate Professor and the Director of Microelectronics Research Laboratory in the Department of Electrical and Computer Engineering, Air Force Institute of Technology, Wright-Patterson Air Force Base, OH (June 1992–December 1997). His research activities include MEMS, silicon micromachining, microsensors, microactuators, optoelectronics, microelectronics, and MEMS packaging. His teaching activities include manufacturing of MEMS, sensor design, and microsystem integration and packaging. From 1995 to 1997, he conducted an AFOSR funded effort into the development of MEMS for low-power optical aberration control. The research resulted in the first successful demonstration of wave front aberration control using a segmented 127 element piston type micromirror array. The results of this work were published in a special issue of *Optical Engineering* (May 1997). During the same period, he also conducted US Air Force sponsored research in multichip module (MCM) packaging of MEMS. This work resulted in the first reported successful packaging of MEMS in commercial MCM packages including ceramic MCM-D, High Density Interconnect (HDI), and Chip on Flex.

Dr. Bright serves on the Executive Committee of the American Society of Mechanical Engineers (ASME) MEMS Sub-Division. He is the Chair of the ASME MEMS Sub-Division Technical Committee for Membership Development and the MEMS Sub-Division representative to the ASME Division of Electrical and Electronic Packaging. Prof. Bright also served on the Technical Committee for IEEE MEMS 2000, IEEE MEMS 2001, and IEEE MEMS 2002 conferences. He received the Best Paper of the MCM'98—Intl. Conference and Exhibition on Multichip Modules and High Density Packaging, Denver, CO, April 15–17, 1998, the Best Paper of Session—International Conference and Exhibition on Multichip Modules and High Density Packaging, Denver, CO, April 15–17, 1998, and the R.F. Bunshah Best Paper Award—1996 International Conference on Metallurgical Coatings and Thin Films.